Synaptopodin is required for efficient intercellular spread by bacterial pathogens.

Short title: Synaptopodin and bacterial infection

Authors: Jenna M. Vickery[1], Jody D. Toperzer[1], Julie E. Raab[1], Desmond J. Hamilton[1], Tucker B. Harju[1], Thao N. Huynh[1], Laurel L. Lenz[1], Liheng Zhou[2], Sean P. Colgan[2], Brian C. Russo[1*]

1. Department of Immunology and Microbiology, University of Colorado School of Medicine, Aurora, CO 80045, USA

2. Division of Gastroenterology and Hepatology, Department of Medicine, University of Colorado School of Medicine, Aurora, CO 80045, USA

*Corresponding author

Email: brian.russo@cuanschutz.edu

Abstract

For many intracellular pathogens, their virulence depends on an ability to spread between cells of an epithelial layer. For intercellular spread to occur, these pathogens deform the plasma membrane into a protrusion structure that is engulfed by the neighboring cell. Although the polymerization of actin is essential for spread, how these pathogens manipulate the actin cytoskeleton in a manner that enables protrusion formation is still incompletely understood. Here, we show that butyrate responsive pathways promote intercellular spread by *Shigella flexneri*. We identify the mammalian actin binding protein synaptopodin, a butyrate responsive gene, as required for efficient intercellular spread of *S. flexneri* and *Listeria monocytogenes*. We show synaptopodin enhances the recruitment of actin to bacteria and stabilizes the actin tail. We show that, for *S. flexneri,* synaptopodin presence enables protrusions to form and to resolve at a greater rate, indicating that greater stability of the actin tail enables the bacteria to push against the membrane with greater force. We demonstrate that synaptopodin recruitment around bacteria requires the bacterial protein IcsA, and we show that this recruitment is further enhanced in a type 3 secretion system dependent manner. These data establish synaptopodin as required for intracellular bacteria to stabilize the actin cytoskeleton in a manner that enables efficient protrusion formation and identify for the first time that synaptopodin contributes to bacterial pathogenesis.

Keywords: Synaptopodin; *Shigella flexneri*; cell-to-cell spread; intercellular spread; intracellular pathogens; IcsA; Spa15; plasma membrane; protrusions; type 3 secretion system; butyrate

42 **Introduction**

43 Many cytosolic-dwelling pathogens recruit actin-associated proteins to enable
44 intercellular spread between mammalian cells (1), including *Listeria* spp*., Rickettsia* spp*.,*
45 *Burkholderia* spp*., Mycobacterium marinum, Shigella* spp*.,* and poxviruses. The forces
46 generated from the polymerization of actin enable their intracellular motility and
47 movement between cells (2, 3). In order to polymerize actin, these organisms subvert
48 preexisting mammalian cytoskeletal pathways. Whereas the ability to repurpose the
49 cellular cytoskeleton is critical for their virulence, the molecular mechanisms that enable
50 actin motility among these pathogens are still incompletely understood (4-6).

51 To gain new insights about how intracellular bacteria spread between cells, we focused
52 on studying the model cytosolic pathogen *Shigella flexneri.* This gram-negative bacterium
53 is a leading cause of bacillary dysentery, a form of bloody diarrhea (6). *S. flexneri* causes
54 disease by invading cells of the colonic epithelium and by spreading between cells in this
55 epithelial layer (7, 8). Cytosolic *S. flexneri* express IcsA at one bacterial pole (9); IcsA
56 binds Neural Wiskott-Aldrich syndrome protein (N-WASP), which then recruits the Actin
57 Related Protein 2/3 complex (Arp2/3) and promotes actin nucleation (10). The
58 polymerization of actin enables the bacteria to move in the cytosol of the cell (11). At the
59 periphery of the cell, some bacteria deform the plasma membrane into a protrusion
60 structure that pushes into the neighboring (recipient) cell (12), where it is actively
61 engulfed. In the recipient cell, these protrusions are resolved into double membrane
62 vacuoles. The bacteria quickly escape the double membrane vacuole into the cytosol,
63 where they can repeat this cycle of intercellular spread (13). Intercellular spread allows
64 the bacterium to access nutrients while evading the immune system, and both the

65 invasion of the colonic epithelium and the spread between cells are essential for
66 pathogenesis (5, 14-17). Defining the molecular mechanisms that promote the
67 intercellular spread of *Shigella* is essential to understand how this organism causes
68 disease.

69 Butyrate is produced by the microbiota and is rapidly metabolized by intestinal epithelial
70 cells (18-20). In these cells, butyrate results in a variety of changes, as it is a potent
71 histone deacetylase (20-22). The pathways regulated by butyrate include a variety of
72 cellular processes, such as energy consumption, hypoxia inducible factors, wound
73 healing, inflammation, and barrier function. We reasoned that many of the targets of
74 butyrate could be relevant during infection and that we could leverage the cellular
75 response to butyrate as a way to uncover new genes and pathways relevant for infection.

76 Here, we show that butyrate promotes *S. flexneri* intercellular spread in intestinal
77 epithelial cells. Based on previous RNAseq studies, we show that synaptopodin, a gene
78 upregulated by butyrate, is important for intercellular spread of *S. flexneri* and *L.*
79 *monocytogenes.* We show protrusion formation and actin tail stability depend on
80 synaptopodin presence. Synaptopodin is recruited to bacteria in a manner that is
81 dependent on the bacterial protein IcsA, and its recruitment is additionally enhanced by
82 a Spa15-dependent bacterial protein. We show that synaptopodin function likely occurs
83 in a manner distinct from previously described pathways. Together, these data, using *S.*
84 *flexneri* as a model, identify synaptopodin as a critical cellular component that enables
85 efficient intercellular spread by cytosolic pathogens.

Results

Synaptopodin is required for efficient intercellular spread by *S. flexneri*.

To identify new proteins and pathways required for intercellular spread, we manipulated cellular function by adding the short chain fatty acid, butyrate, to the culture media. We compared the effect of butyrate on the efficiency of spread for *S. flexneri* through a monolayer of human colonic adenocarcinoma epithelial (T84) cells using a plaque assay. In this assay, infected cells are killed by the bacteria as they spread, creating clearings in the monolayer, known as “plaques”. The number of plaques is a function of the efficiency of invasion, and the area of the plaque is a function of the efficiency of intercellular spread. We observed larger plaques in the presence of butyrate (Fig. 1A-B), demonstrating butyrate enables more efficient spread by *S. flexneri* in these cells. On its own, butyrate did not change the replication of *S. flexneri* (Fig. S1), suggesting that the increased efficiency of spread is independent of bacterial replication and that butyrate may alter cellular pathways necessary to promote intercellular spread.

Previous RNA sequencing of T84 cells identified genes whose expression was altered by butyrate and identified Synaptopodin (23). We show that butyrate caused a 3-fold increase in synaptopodin protein in our assays (Fig. 1C-D). Synaptopodin is an actin binding protein that alters the efficiency of actin polymerization and interacts with cell-cell junction proteins. Its robust induction by butyrate, its subcellular localization at sites of intercellular spread, and its regulation of actin-dependent processes indicated that synaptopodin could have roles during *S. flexneri* intercellular spread.

107 To investigate this, a control or synaptopodin specific shRNA was introduced into
108 T84 cells, and the efficiency of intercellular spread was determined by a plaque assay.
109 Synaptopodin protein abundance was reduced in the presence of the synaptopodin-
110 specific shRNA (23), and *S. flexneri* formed smaller plaques in Synpo knockdown cells
111 compared to control cells (Fig. 2A-B). These data suggest that synaptopodin promotes
112 intercellular spread by *S. flexneri*.

113 The effect of synaptopodin on intercellular spread was not specific to T84 cells;
114 plaques were significantly smaller in Madin-Darby canine kidney (MDCK) cells producing
115 a control shRNA compared to MDCK cells producing a synaptopodin-specific shRNA (Fig.
116 2C-D). Synaptopodin was efficiently knocked-down in these cells [Fig. S2A-B, (23, 24)].
117 The ability of *S. flexneri* to spread through monolayers of HeLa cells producing a control
118 shRNA or one of five synaptopodin-specific shRNAs was also investigated. Plaques
119 formed in monolayers of HeLa cells producing four of the five synaptopodin-specific
120 shRNAs were smaller than plaques formed in cells producing the control shRNA (Fig. 2E-
121 F and S2C-D). The four cell lines displaying reduced plaque size also demonstrated a
122 reduction in synaptopodin protein level (Fig. S2E-F). Thus, the smaller plaque size
123 observed above was unlikely the result of non-specific effects of an individual shRNA. *S.*
124 *flexneri* replicated at a similar efficiency in T84, MDCK, and HeLa cells that produced or
125 lacked synaptopodin (Fig. S2G-L), indicating that the impact of synaptopodin on plaque
126 size is not due to differences in bacterial replication. Moreover, since similar results were
127 observed in T84, MDCK, and HeLa cells, these data indicate that the requirement of
128 synaptopodin for *S. flexneri* spread is unlikely to be specific for a particular cell type.

129 *L. monocytogenes* is a gram-positive bacterium that, like *S. flexneri,* requires actin-
130 based motility for intercellular spread (25). The ability of *L. monocytogenes* to spread
131 through a monolayer of HeLa cells producing a control shRNA was compared to its ability
132 to spread through cells producing a synaptopodin-specific shRNA by fluorescence
133 microscopy. Similar to the observations with *S. flexneri,* plaques formed by *L.*
134 *monocytogenes* were larger in the presence of synaptopodin (Fig. S3), demonstrating
135 that synaptopodin is required for intercellular spread of *Listeria*. Together, these data
136 show that *S. flexneri* and *L. monocytogenes* require synaptopodin for efficient intercellular
137 spread and indicate the requirement for synaptopodin may be a general feature of
138 intracellular bacterial pathogens that spread.

139 **Synaptopodin is required for protrusion formation by *S. flexneri***

140 To investigate how synaptopodin contributes to efficient intercellular spread, we
141 focused on aspects of the bacterial intracellular life cycle that require actin. We assessed
142 the ability of bacteria to form plasma membrane protrusions in HeLa cells producing either
143 a control or a synaptopodin-specific shRNA. We determined the percentage of bacteria
144 present in a protrusion at 90 minutes of infection by examining the manner of actin
145 polymerized at the posterior pole of bacteria by immunofluorescence microscopy. We
146 performed similar studies in which a membrane-anchored YFP was introduced into cells
147 and used to mark the plasma membrane. For both approaches, a smaller percentage of
148 bacteria in synaptopodin knockdown cells were present in plasma membrane protrusions
149 compared to the percentage of bacteria in protrusions in control cells (Fig. 3A-B and S4),
150 demonstrating that synaptopodin is required for efficient protrusion formation.

151 Synaptopodin is associated with the bundling and elongation of actin filaments in
152 cells (26, 27), but actin intensity at the plasma membrane near protrusions was similar in
153 the presence and absence of synaptopodin (Fig. 3C), indicating that the protrusion defect
154 is not due to defects in the amount of actin recruited to protrusions. Protrusion formation
155 is also dependent on actin that is polymerized by formins. The formin mDia1 is required
156 for formation of protrusions by *S. flexneri* and *L. monocytogenes* (28, 29). mDia1 was
157 efficiently recruited to protrusions formed in control or synaptopodin knockdown cells (Fig.
158 S5), indicating reduced mDia1 levels around bacteria are not driving the reduction in
159 protrusion formation in the relative absence of synaptopodin. The length of the protrusion
160 is more generally associated with the efficiency of intercellular spread (30). Protrusion
161 lengths were similar irrespective of synaptopodin levels in HeLa cells (Fig. 3D), indicating
162 that the requirement for synaptopodin was not associated with protrusion length.

163 We next investigated the kinetics of protrusion formation by *S. flexneri* to further
164 clarify the role of synaptopodin in the development of membrane protrusions. To visualize
165 the formation of protrusions, intracellular bacteria were tracked by time-lapsed
166 microscopy during infection of HeLa cells that produce a YFP that is anchored to the
167 plasma membrane (31). Bacteria in control cells formed protrusions at a greater velocity
168 than bacteria in cells lacking synaptopodin (Fig. 3E-F). Protrusions formed in the
169 presence of synaptopodin were also faster to resolve, lasting an average of 18 min in
170 control cells compared to 27 min in synaptopodin knockdown cells (Fig. 3G). These data
171 show synaptopodin enables more rapid formation and resolution of protrusions.

172 **Synaptopodin regulates actin tail formation by *S. flexneri***

173 The ability to efficiently assemble an actin tail in the cell cytosol is associated with
174 efficient protrusion formation at the plasma membrane (32). We hypothesized that the
175 defects in protrusion formation were the result of aberrant actin tail formation. To test this,
176 we infected HeLa cells with *S. flexneri* and characterized the actin tails. Although a similar
177 percentage of bacteria formed actin tails in the control and synaptopodin knockdown cells
178 (Fig. 4A-B), actin tails that formed in the synaptopodin knockdown cells were significantly
179 shorter than actin tails in the control cells (Fig. 4C). In MDCK cells, the actin tails formed
180 by *S. flexneri* in the control cells were also significantly longer than tails in the
181 synaptopodin knockdown cells (Fig. S6A-B). Previous studies have shown that the length
182 of the actin tails correlates with the rate of actin polymerization and the speed bacteria
183 move in the cytosol (33). Since we observed shorter tails in HeLa and MDCK cells, it
184 suggested to us that the rate of actin polymerization could be reduced in the absence of
185 synaptopodin and would result in *S. flexneri* moving more slowly through the cytosol of
186 cells. To test this, time-lapsed microscopy was performed on intracellular bacteria in HeLa
187 cells to evaluate the efficiency of actin-based motility. In contrast to our expectation based
188 on the length of the actin tails, the bacterial velocity was similar in the control and
189 synaptopodin knockdown cells (Fig. 4D-E). Since bacteria were moving at a similar
190 speed, it suggested that the rate of actin polymerization was similar in the presence and
191 absence of synaptopodin and indicated that synaptopodin stabilizes the polymerized actin
192 tail resulting in longer actin tails in the control cells.

193 In addition to differing in length, the width of the actin tails at the base of the
194 bacteria was wider in control HeLa cells than in synaptopodin knockdown HeLa cells (Fig.
195 S7A-B). Interestingly, actin tails at the base of the bacteria in MDCK cells were not

196 significantly different in width between control and synaptopodin knockdown cells (Fig.
197 S6C). We also noted additional phenotypic changes to the tails in HeLa cells lacking
198 synaptopodin. Polymerized actin was more frequently present along the lateral sides of
199 the posterior end of bacteria in the control cells compared to in synaptopodin knockdown
200 cells (Fig. S7C). During bacterial infection or when examining actin polymerization around
201 lipid vesicles, the actin on the sides of the bacteria or vesicle creates an inward force at
202 the base that is predicted to contribute to the propulsive force (34, 35). Seeing that there
203 was no difference in the velocity at which *S. flexneri* traveled whether or not actin
204 extended along the sides of the bacteria, we hypothesized that the additional actin may
205 stabilize the tail and keep the actin tail in line with the bacteria, which we anticipated would
206 stabilize the path along which the bacteria travels. To investigate this, we measured the
207 angle at which the actin tail extended from the posterior pole of the bacteria. We set actin
208 tails that formed completely in line with the longitudinal axis of the bacteria at 0° and
209 deviations from this alignment resulted in an increased angle. In the synaptopodin
210 knockdown cells, the actin tails were less aligned with the bacteria's longitudinal axis than
211 the tails associated with bacteria in the control cells, which resulted in a greater angle
212 from the longitudinal axis for bacteria in synaptopodin knockdown cells (Fig. S7D). These
213 data show that synaptopodin enables actin presence along the lateral sides near the
214 posterior end of the bacteria and that synaptopodin enables the actin tail to be more in
215 line with the bacteria. We theorized that the angle of the actin tail would decrease the
216 forward momentum that the actin nucleation creates at the base of the bacteria. We used
217 the formula, [*sin (angle of the tail(θ)) + cos (angle of the tail(θ))*], to calculate the total force
218 of the actin tail on the bacteria. We then calculated the percentage of force that

219 contributed to the forward momentum of the bacteria by the formula, [*(cos (angle of the*
220 *tail(θ)) / total force) * 100*]. The percentage of the theoretical forward movement of
221 bacteria in the control cells is higher than in the synaptopodin knockdown cell lines (Fig.
222 S7E). We hypothesized that the defects in the actin tail length, width, organization, and
223 angle of attachment would lead to a defect in the linear trajectory of the bacteria in the
224 absence of synaptopodin. We tracked intracellular bacteria with time-lapsed microscopy
225 to evaluate the linear trajectory. We calculated the distance an individual bacteria traveled
226 and divided it by the distance of the theoretical most efficient path – a straight line. A
227 bacterium that took the most efficient path would have a linear trajectory ratio of 1.0. We
228 observed that bacteria deviated further from an ideal path in cells lacking synaptopodin
229 compared to control cells (Fig. S7F), which showed that bacteria traveled along a
230 straighter path in the presence of synaptopodin.

231 We asked whether the defects associated with the actin tails were specific to *S.*
232 *flexneri* or a more general result of pathogens that spread between cells with lower levels
233 of synaptopodin. We tested whether the length of actin tails was similarly decreased
234 during *L. monocytogenes* infection of HeLa cells. Similar to *S. flexneri,* actin tails formed
235 by *L. monocytogenes* were longer in the presence of synaptopodin compared to the actin
236 tails formed in the absence of synaptopodin (Fig. S8).

237 Altogether, these data show that synaptopodin presence stabilizes polymerized
238 actin tails resulting in longer actin tails and that, in HeLa cells, synaptopodin additionally
239 enables actin accumulation at the bacterial pole in a manner that generates more directed
240 forward momentum.

241 **Synaptopodin colocalizes around *S. flexneri***

242 Based on the requirement for synaptopodin in organizing the actin tail and in
243 forming protrusions, we hypothesized that *S. flexneri* would recruit synaptopodin to its
244 pole during intracellular infection. To test this, we infected HeLa and MDCK cells with *S.*
245 *flexneri* and used immunofluorescence microscopy to visualize synaptopodin localization
246 in cells. Synaptopodin was recruited to bacteria in the cytosol (Fig. S9A-C and S10). This
247 recruitment of synaptopodin mirrored that of actin and was observed at the poles, the
248 lateral sides of the bacteria, or both. Furthermore, synaptopodin localizes to bacteria that
249 also displayed actin recruitment, but synaptopodin was not observed around bacteria that
250 failed to recruit actin (Fig. S9-S10). These data show that synaptopodin is recruited to
251 bacteria that nucleate actin polymerization.

252 Knockdown of synaptopodin caused fewer bacteria to recruit synaptopodin (Fig.
253 S9A-B), and among the bacteria that showed synaptopodin recruitment, there was a
254 reduction in the intensity of synaptopodin (Fig. S9C). Although loss of synaptopodin did
255 not reduce the percentage of bacteria that formed an actin tail (Fig. 4B), the knockdown
256 of synaptopodin significantly reduced the number of bacteria that recruited actin (Fig.
257 S9D), yet there was not a significant difference in the intensity of the actin signal among
258 the bacteria that recruited actin in the presence or absence of synaptopodin in these
259 experiments (Fig. S9E). These data show that synaptopodin is recruited to the poles and
260 sides of intracellular bacteria that polymerize actin and synaptopodin presence enhances
261 the number of bacteria that recruit actin.

262 **Synaptopodin promotes myosin IIb recruitment around *S. flexneri*.**

263 The localization of IcsA to the posterior pole of *S. flexneri* results in the recruitment
264 of N-WASP and the Arp2/3 complex and enables the initiation of actin polymerization and
265 bacterial motility (10). Synaptopodin is known to regulate this process through another
266 protein Nck1 (36). Synaptopodin promotes Nck1 abundance in cells by blocking c-Cbl-
267 mediated ubiquitination of Nck1, and Nck1 assists in N-WASP and Arp2/3 recruitment
268 during vaccina virus infection (36, 37). We tested whether the defect in actin recruitment
269 in cells lacking synaptopodin was due to a disruption in this synaptopodin-Nck1-Arp2
270 pathway. We observed a similar percentage of bacteria that recruited Arp2, and these
271 bacteria were associated with similar levels of Arp2 as measured by the intensity of the
272 fluorescent signal of Arp2 around bacteria (Fig. S11A-C). We tested whether Nck1 was
273 recruited to the bacteria during intracellular infection. We found no evidence of Nck1
274 recruitment in our cells (Fig. S11D). We examined the ability of *S. flexneri* to recruit N-
275 WASP and observed a similar percentage of bacteria recruited N-WASP (Fig. S11E-F).
276 Among the bacteria that recruited N-WASP, the amount of N-WASP was similar
277 irrespective of synaptopodin levels (Fig. S11G). Consistent with our findings above that
278 Synaptopodin likely stabilizes the polymerized actin in the tail rather than altering the rate
279 of actin polymerization, here, we did not see defects in the recruitment of key proteins
280 required to intiate actin polymerization at the posterior pole of the bacteria.

281 We further sought to examine whether we could identify interactions that were
282 important for the formation of the protrusion. Synaptopodin is described to interact with
283 non-muscle myosin IIb (myosin IIb) and α-actinin-4 at the plasma membrane, where
284 together they form the contractomere complex that generates force so as to enable the
285 extrusion of cells from a monolayer (24). Recent work shows that α-actinin-4 is present

286 at actin structures formed during *S. flexneri* infection (1). We tested for the recruitment of
287 myosin IIb and α-actinin-4 by immunofluorescence microscopy, and observed both were
288 efficiently recruited to *S. flexneri.* Interestingly, a smaller percentage of bacteria recruited
289 myosin IIb in the absence of synaptopodin (Fig. 5A-B), but among the bacteria that
290 recruited myosin IIb, there was a similar abundance of myosin IIb as measured by
291 fluorescent intensity irrespective of synaptopodin levels (Fig. 5C). We observed similar
292 levels of α-actinin-4 recruited to bacteria and similar abundance of α-actinin-4 around the
293 bacteria as measured by fluorescent intensity in control and synaptopodin knockdown
294 cells (Fig. 5D-F). Altogether, these data indicate that synaptopodin presence enhances
295 myosin IIb recruitment around *S. flexneri*.

296 **IcsA and the type 3 secretion system regulate synaptopodin recruitment around *S.***
297 ***flexneri.***

298 *S. flexneri* requires a type three secretion system (T3SS) for intercellular spread (38-40).
299 This type 3 secretion system delivers over 30 bacterial virulence proteins (effectors) into
300 the cell (41). The delivered effectors coopt cellular signaling pathways and enable *S.*
301 *flexneri* to thrive in the intracellular environment. Here, we sought to determine whether
302 synaptopodin was recruited around the bacteria indirectly due to the high concentrations
303 of polymerized actin around the bacteria, as a result of direct recruitment by *S.*
304 *flexneri* secreted proteins, or both. To do so, we tested whether IcsA or the type 3
305 secreted effector proteins contributed to synaptopodin recruitment by investigating
306 synaptopodin localization during cellular infection by several bacterial mutants: *S. flexneri*
307 △*icsA* is unable to polymerize actin; *S. flexneri* △*spa15* lacks a chaperone for nine type 3

308 secreted effector proteins – the absence of Spa15 results in these proteins being unstable
309 and degraded (42); *S. flexneri* △*mxiE* lacks the MxiE transcription factor that is necessary
310 to transcriptionally activate the expression of more than 25 effectors – in the absence of
311 MxiE these effectors are not produced in the bacteria (43-45). Together, the absence of
312 Spa15 and MxiE enabled us to examine whether more than 30 effectors contribute to
313 synaptopodin recruitment as two pooled groups. We infected HeLa cells with these
314 mutants and quantified the percentage of bacteria that showed recruitment of
315 synaptopodin and/or actin, and we measured the intensities of these recruited proteins.
316 As expected, *S. flexneri* △*icsA* did not recruit actin or form actin tails during intracellular
317 infection (Fig. 6A-B). Interestingly, bacteria lacking IcsA also did not recruit synaptopodin
318 (Fig. 6C). A similar percentage of wild-type bacteria and bacteria lacking MxiE recruited
319 actin and synaptopodin (Fig. 6A-C). Loss of Spa15 resulted in a smaller percentage of
320 bacteria that recruited actin compared to wild-type bacteria, but a similar percentage of
321 wild-type and Spa15 deficient bacteria recruited synaptopodin (Fig. 6C). When we
322 examined the amount of actin and synaptopodin recruited around bacteria by comparing
323 the intensity of fluorescent signal, we observed that except for the *icsA* mutant, actin was
324 efficiently recruited around bacteria (Fig. 6D). Yet, when we examined the amount of
325 synaptopodin around bacteria, we observed that bacteria lacking Spa15 or IcsA recruited
326 less synaptopodin than wildtype bacteria (Fig. 6E). Altogether these data show that
327 bacterial recruitment of synaptopodin is dependent on *S. flexneri* protein IcsA and is
328 enhanced in a type 3 secretion-dependent manner.

329 **Discussion**

330 Many cytosolic-dwelling pathogens require the subversion of actin and host
331 proteins for intracellular motility. These pathogens remodel the cytoskeleton and plasma
332 membrane resulting in the formation of protrusions, which facilitate intercellular spread.
333 Here, we show that butyrate responsive pathways enhance *S. flexneri* intercellular
334 spread. We identify that the butyrate responsive protein synaptopodin promotes *S.*
335 *flexneri* and *L. monocytogenes* intercellular spread. We show that synaptopodin function
336 is required to stabilize actin tails and to promote efficient protrusion kintecs, and we show
337 that synaptopodin is recruited to bacteria in a manner that is dependent on the bacterial
338 protein IcsA and the type 3 secretion system. Thus, these findings identify that bacterial
339 pathogens, such as *S. flexneri* and *L. monocytogenes,* drive changes in the subcellular
340 localization of synaptopodin in a manner that promotes actin tail stability, protrusion
341 formation, and intercellular spread (Fig. 7).

342 Here, we used butyrate as a tool to manipulate epithelial cell function. Whereas it
343 is unclear whether this short chain fatty acid would have direct effects on intercellular
344 spread during intestinal infection, there is reason to belive that *S. flexneri* infection would
345 create conditions where butyrate responsive pathways in epithelial cells are relevant for
346 spread. Butryate treatment is known to stabilize hypoxia indicble factor 1a (HIF1a) (22,
347 46). HIF is degraded under normoxia, but is stabilized and active under hypoxic
348 conditions. *S. flexneri* infection is known to create hypoxic conditions in the intestinal
349 epithelium (47, 48). Moreover, the stabilization of HIF is associated with increased levels
350 of synaptopodin. We speculate that a consequence of *S. flexneri* induced hypoxia is the

351 stabilization of HIF and upregulation of synaptopodin such that intercellular spread
352 becomes more efficient.

353 Previous studies have shown that the length of the actin tail formed by *L.*
354 *monocytogenes* directly correlates with the rate of actin polymerization and the
355 intracellular velocity of the bacteria (33). Although synaptopodin presence enabled longer
356 actin tails to form (Fig. 4C, S6, and S8), synaptopodin loss did not alter the speed the
357 bacteria moved in the cytosol (Fig. 4D-E). Moreover, proteins associated with actin
358 nucleation, such as N-WASP and Arp2, were efficiently recruited to bacteria irrespective
359 of synaptopodin (Fig. S11A-C and E-G). These findings suggest that rather than altering
360 the rate of actin polymerization, synaptopodin stabilizes the actin filaments that are
361 already formed leading to the generation of longer actin tails. Similar to our findings, the
362 stabilization of F-actin by synaptopodin enables the formation of dendritic spines in
363 neurons (27, 49). Although the bacterial velocity is associated with actin monomer
364 addition in the cytosol, it is likely that the rate of addition of new actin monomers as well
365 as the rate of loss of old actin monomers may both contribute to the speed at which the
366 protrusions form. Consistent with our model, the tail length did not correlate with bacterial
367 speed in the cytosol, but was asocciated with a decreased rate of protrusion formation in
368 the absence of synaptopodin (Fig. 3F).

369 Along with shorter actin tails, bacterial tails formed in the synaptopodin knockdown
370 HeLa cells were less aligned with the longitudinal axis of the bacteria and lacked actin
371 recruitment along the sides of the bacteria. Here, our data indicate that the additional
372 actin provides a stabilizing effect by maintaining actin polymerization in line with the
373 bacterial longitudinal axis and enabling the bacteria to move in a more directed manner

374 forward (Fig. S7F). In MDCK cells, synaptopodin was associated with decreased length
375 of actin tails, but not the width (Fig. S6). Our data indicate that a reduction of actin on the
376 sides of the bacteria does not affect the velocity of cytosolic bacteria (Fig. 4). Rather, we
377 speculate that this specific synaptopodin-dependent localization of actin in HeLa cells
378 may be necessary at the membrane where the bacteria experience additional forces
379 during the formation of the protrusion.

380 Previous studies have shown that synaptopodin forms a force-generating complex
381 with α-actinin-4 and myosin IIb that pulls from the pointed-end toward the barbed-end of
382 the actin filaments. This force generation results in the buckling of actin filaments and
383 pulls on the plasma membrane in a manner that causes cells to extrude from a monolayer
384 (24). One role for synaptopodin could be to function as a force-generating complex that
385 pushes actin filaments into the protrusion structure and enables protrusion formation to
386 be more efficient, but we anticipate this is unlikely to occur during infection. The barbed
387 end of the filaments would be proximal to the bacteria where the incorporation of new
388 actin monomers occurs. Thus, force generation by synaptopodin as described for the
389 contractomere complex would generate a resistive force against protrusion formation by
390 pulling the barbed end of actin back into the cell rather than pushing them out of the cell.
391 Yet, we observe protrusions form faster with synaptopodin (Fig. 3E-G). An intriguing
392 possibility is that synaptopodin, as part of the contractomere complex, is anchored at the
393 plasma membrane and pulls the membrane along the actin filaments toward the bacteria.
394 By pulling membrane into the protrusion, the contractomere complex would both create
395 some slack in the membrane so as to enable the bacteria to more efficiently form the
396 protrusion structure and would provide some mechanism for how the significant amount

397 of plasma membrane is redirected into the protrusion. Although we have not seen
398 previous descriptions of myosin IIb associating with bacteria during *S. flexneri* infection,
399 previous reports do indicate roles for myosin IIa and myosin X (30, 50), and we
400 hypothesize that myosin IIb could function in a similar manner by pulling the plasma
401 membrane into the protrusion (30). A second possibility is that the presence of
402 synaptopodin simply stabilizes the actin fibers, as described above, so that the loss of
403 actin monomers is less efficient and the fibers remain longer in the protrusion for a greater
404 period of time, thereby promoting the formation of the protrusion structure.

405 *Shigella* spp., *Listeria* spp., *Rickettsia* spp., *Burkholderia* spp., *Mycobacterium*
406 *marinum,* and pox viruses such as vaccina virus are all examples of pathogens that
407 require actin nucleation for their virulence. Recent studies show that mitochondria use
408 similar mechanisms of motility by generating actin comet tails so as to enable organelle
409 segregation during mitosis (51). Our findings show that synaptopodin is a critical regulator
410 of actin polymerization and organization during *S. flexneri* and *L. monocytogenes*
411 intercellular spread, and we anticipate that our findings represent a more general role of
412 synaptopodin-dependent regulation of actin dynamics in cells and during infection.

413 **METHODS**:

414 **Bacterial Culture:**
415
416 *S. flexneri* strain 2457T is used in this study; all mutants are isogenic to it (8). *S. flexneri*
417 strains were cultured in trypticase soy broth (TCS) at 37°C and at 250 rpm. Bacteria were
418 transformed with pROEX-Aqua [Addgene; plasmid #42889, (52)] or pBR322-mCherry for
419 live and fixed microscopy. *L. monocytogenes* strain 10403S is used in this study (53). *L.*
420 *monocytogenes* strains were cultured in trypticase soy broth (TCS) at 37°C.

421 **Cell Culture:**

422 HeLa cells, MDCK cells (gift of Vivian Tang), and T84 cells were maintained at 37°C in
423 5% CO_2. HeLa and MDCK cells were grown in Dulbecco's modified Eagle's Medium
424 (DMEM) supplemented with 10% fetal bovine serum (FBS). T84 cells were grown in
425 Advance DMEM supplemented with 10% FBS and 1% L-glutamine. The generation of
426 cells producing control or synaptopodin specific shRNA were previously described for T84
427 cells (23) and MDCK cells (24). HeLa cells producing shRNA targeting synaptopodin were
428 generated using retroviral transduction followed by selection with 5 µg/mL puromycin.

429 **Virus Preparation:**

430 3 million 293T cells were seeded in 100 mm dishes in DMEM supplemented with 10%
431 FBS for 24 hours prior to transduction. Cells were transduced with psPAX2 (Addgene,
432 12260), pVSVg, and either pLKO.5 (SHC216) for control shRNA or a synaptopodin
433 specific shRNA (TRCN0000218429, TRCN0000230911, TRCN0000230913,
434 TRCN0000230912, TRCN0000218782), or pmbYFP (Gift of Hervé Agaisse). Plasmids

435 were transfected into cells using calcium phosphate. The next day, the media was
436 replaced with fresh DMEM supplemented with 10% FBS. After incubation for an additional
437 24 hours, the culture supernatant containing the viral particles was collected, passed
438 through a 0.45 µm filter, and stored at -20°C.

439 **Viral Transduction:**

440 3 x 10^5 HeLa cells in 6-well plates were treated with 2 mL of filtered 293 supernatant
441 containing 4mM polybrene and centrifuged for 2 hours at 1000 *g* at 30°C. Cells were
442 incubated at 37°C for 48 hours, and then treated with 5 µg/mL puromycin. Resistant cells
443 were expanded. For cells additionally transduced with virus encoding the membrane
444 anchored YFP, cells were sorted at the Flow Cytometry Shared Resource Laboratory in
445 the Department of Immunology and Microbiology to enrich for YFP positive cells.

446 **Plaque Assay:**

447 8 x 10^5 cells per well were seeded in 6-well plates. The next day, cells were infected with
448 *S. flexneri* at a multiplicity of infection (MOI) of 0.2 for HeLa cells or a MOI of 20 for MDCK
449 cells and T84 cells. Bacteria were centrifuged onto cells at 800 *g* for 10 minutes and
450 incubated at 37°C in 5% CO_2 for 90 min. Media was replaced with DMEM containing 10%
451 FBS, 25 µg/mL gentamicin, and 0.5% agarose, and the cells were incubated for 48 hours.
452 To visualize plaques, a second overlay was added with 0.7% agarose in DMEM with 10%
453 FBS, 25 µg/mL gentamicin, 0.1% neutral red. Following incubation for at least 4 hours,
454 the plates were imaged with an ImmunoSpot S6 Universal Visible/Fluorescent Analyzer
455 (Cellular Technology Limited). Analysis of the plaque area was performed using a pipeline
456 generated in ImageJ in which images were thresholded to remove background, pixel

457 intensity was converted to a binary, and the images were segmented into objects; objects
458 matching plaques on unmodified images were selected, and their area was quantified, as
459 done previously (39). For experiments with butyrate, 5 mM butyrate was added 1 hour
460 prior to infection and maintained throughout the infection.

461 **Spread Assay by Microscopy:**

462 Cells were seeded at 7 x 10^5 cells per well in 6-well plates onto sterile coverslips. The
463 next day, cells were infected with *L. monocytogenes* at a MOI of 15. The bacteria were
464 centrifuged onto cells at room temperature at 800 *g* for 10 minutes. The co-culture was
465 incubated at 37°C with 5% CO_2 for 45 mins. Cells were washed and remaining
466 extracellular bacteria were killed by DMEM supplemented with 10% FBS and 25 µg/mL
467 gentamicin. The infection was incubated for an additional 24 hours and fixed with 3.7%
468 paraformaldehyde. The cells were permeabilized with 1% triton X-100 in PBS and washed
469 five times with PBS. Cells were stained with phalloidin conjugated to Alexa Flour 750
470 (Invitrogen A30105), washed with PBS, stained with Hoechst 33342 (Biotech No. 5117),
471 washed twice with PBS, and mounted with Prolong Diamond Antifade Mountant
472 (ThermoFisher, P36930). Images were taken at random at 20x magnification. Five fields
473 of view were analyzed per condition per experiment and area of spread was measured
474 with NIS elements.

475 **Quantification of Intracellular Bacteria:**

476 T84 cells were seeded at 8 X 10^5 cells per well, and HeLa or MDCK cells were seeded at
477 4 X 10^5 cells per well in a 6-well plate. The next day, cells were infected with *S. flexneri*
478 at an MOI of 200, by centrifugation at at 800 *g* for 10 minutes. The co-culture was

479 incubated at 37°C with 5% CO_2 for 45 minutes. Excess bacteria were removed by three
480 washes with HBSS. Extracellular bacteria were killed by DMEM supplemented with 10%
481 FBS and 25 µg/mL gentamicin. The infection was incubated for an additional 1, 2, or 3
482 hours. The cells were washed three times with HBSS, and then the cells were lysed with
483 0.02% SDS in HBSS. The cell lysates with intact bacteria were serially diluted in TCS
484 broth and plated onto TCS agar to determine the intracellular CFU.

485 **Western Blots:**

486 SDS-PAGE gels were transferred to nitrocellulose using a Turbo semi dry transfer
487 apparatus (BioRad). For detection of antigen, 1:100 rabbit anti-synaptopodin (Abcam,
488 ab224491) was incubated overnight at 4°C in 5% milk. The next day, blots were incubated
489 at room temperature with 1:5,000 goat anti-rabbit (Jackson Immuno Research Labs, 111-
490 035-144) for 2 hours or 1:10,000 anti-β-actin conjugated to HRP (Sigma A3854) for 1
491 hour. Western blots were developed, and the signal was acquired by a G:Box (Syngene).
492 Band intensity was measured using ImageJ (NIH) with the background subtracted.

493 **Localization of Host Proteins:**

494 HeLa cells or MDCK cells were seeded at 8 X 10^5 cells per well in a 6-well plate and
495 cultured for 24 hours (HeLa) or 48 hours (MDCK). Cells were infected with designated
496 strains of *S. flexneri* harboring pROEX-Aqua by centrifugation at 800 *g* for 10 minutes
497 and incubated at 37°C in 5% CO_2. At 45 minutes of infection, cells were washed three
498 times with HBSS, and media was replaced with DMEM with 10% FBS, 25 µg/mL
499 gentamicin, and 100 mM IPTG. After an additional 45 minutes, cells were fixed with 3.7%
500 paraformaldehyde. The cells were permeabilized with 1% triton X-100 in PBS for 30

501 minutes at room temperature. The cells were washed five times with PBS and incubated
502 in PBS with 10% FBS and 1:100 rabbit anti-synaptopodin (Abcam, ab224491), 1:1000
503 rabbit anti-N-WASP (Santa Cruz Biotechnology Inc, sc100964), 1:500 rabbit anti-α-
504 actinin-4 (Abcam, ab108198), 1:50 rabbit anti-mDia1 (Abcam, AB129167), 1:500 mouse
505 anti-myosin IIb (Santa Cruz Biotechnology Inc, sc-376942), or 1:50 goat anti-Arp 2 (Novus
506 Biologicals, NB100-1037) overnight at 4°C. The cells were washed with PBS, incubated
507 with 1:100 donkey anti-rabbit-Alexa Fluor 594 (ThermoFisher, A-21207), goat anti-rabbit-
508 Alexa Fluor 750 (ThermoFisher, A21039), donkey anti-mouse-Alexa Fluor 594
509 (Invitrogen, A32744), or donkey anti-goat-Alexa Fluor 594 (ThermoFisher, A32758) for 2
510 hours at room temperature, and washed with PBS. Cells were stained with phalloidin-
511 Alexa Flour 750 (Invitrogen A30105) or Alexa Fluor 647 (Invitrogen, A22287), washed
512 with PBS, stained with Hoechst 33342 (Biotech No. 5117), washed twice with PBS, and
513 mounted with Prolong Diamond Antifade Mountant (ThermoFisher, P36930).

514 **Live Imaging for Speed of Cytosolic Bacteria and of Protrusion Formation:**

515 HeLa cells expressing a membrane-anchored yellow fluorescent protein were seeded at
516 8 X 10^5 cells per well on Ibidi 2-well chamber slides (Ibidi, 80286). The next day, cells
517 were infected with designated strains of *S. flexneri* harboring the pROEX-Aqua plasmid
518 at an MOI of 400 by centrifugation at 800 x*g* for 10 minutes. At 1 hour of infection, cells
519 were washed with HBSS 10 times, and media was replaced with DMEM supplemented
520 with 10% FBS, 25 µg/mL gentamicin, and 100 mM IPTG. A time-lapsed Z-stack of images
521 was collected with a Nikon Eclipse Ti-2 inverted light microscope at 37°C and 5% CO_2 at
522 10-second intervals for 10 minutes. Images were deconvolved using a Richardson-Lucy
523 algorithm with 20 iterations and all slices within a stack were collapsed into a single image

524 based upon the maximum intensity of pixels in each slice using NIS elements software.
525 For time-lapsed series, in which some focal drift occurred in the XY position, FIJI plugin:
526 Linear Stack Alignment with SIFT, was used to realign timepoints. NIS elements particle
527 tracking software was used to track in-frame bacteria throughout the video to calculate
528 protrusion velocities. Speed was determined for each bacterium by measuring the
529 distance traveled over the duration of time bacterium was in focus.

530 **Live-cell Imaging Analysis for Protrusions Duration:**

531 HeLa cells expressing a membrane-anchored yellow fluorescent protein were seeded at
532 2 X 10^5 cells per well on Ibidi 8-well chamber slides (Ibidi, 80826). The next day, media
533 was replaced with DMEM and 10% FBS and cells were infected with designated strains
534 of *S. flexneri* expressing mCherry at an MOI of 200. At 1 hour of infection, cells were
535 washed with HBSS 10 times, and media was replaced with DMEM supplemented with
536 10% FBS. A time-lapsed Z-stack of images was taken with a Nikon Eclipse Ti-2 inverted
537 light microscope at 37°C and 5% CO_2 at 5-minute intervals for 2.5 hours to examine
538 protrusion duration. Images were deconvolved using a Richardson-Lucy algorithm with
539 20 iterations and all slices within a stack were collapsed into a single image based upon
540 the maximum intensity of pixels in each slice using NIS elements software. Protrusion
541 duration was measured by quantifying the amount of time the bacteria were in each
542 protrusion stage (54).

543 **Quantification of the length of actin tails formed by *L. monocytogenes***

544 HeLa cells were seeded at 8 X 10^5 cells per well in a 6-well plate and cultured for 24
545 hours. The next day, cells were infected with *L. monocytogenes* harboring pGFP (55) at

546 an MOI of 1,500. Bacteria were centrifuged onto cells at 800 *g* for 10 minutes and
547 incubated at 37°C in 5% CO_2. At 90 minutes of infection, cells were washed three times
548 with HBSS, and media was replaced with DMEM with 10% FBS and 25 µg/mL gentamicin.
549 After an additional 3.5 hours, cells were fixed with 3.7% paraformaldehyde for at least 20
550 minutes at room temperature. The cells were permeabilized with 1% triton X-100 in PBS
551 for 30 minutes at room temperature. The cells were washed 5 times with PBS. Cells were
552 stained with phalloidin conjugated to Alexa Flour 750 (Invitrogen A30105), washed with
553 PBS, stained with Hoechst 33342 (Biotech No. 5117), washed twice with PBS, and
554 mounted with Prolong Diamond Antifade Mountant (ThermoFisher, P36930).

555 **Microscopy:**

556 Fluorescent images were acquired on a Nikon Eclipse Ti-2 inverted light microscope
557 equipped with an Orca Fusion BT cMOS camera (Hammamatsu), an IRIS 15 cMOS
558 camera (Photometrics), Semrock Brightline filters, and an Oco stage top incubator
559 chamber that enables regulation of temperature, CO_2, and humidity. NIS elements
560 software (Nikon) was used for image acquisition and analysis. Images were deconvolved
561 using a Richardson-Lucy algorithm with 20 iterations. Microscopic images were pseudo-
562 colored and assembled using Adobe photoshop or FIJI (NIH). Images were collected
563 randomly across the coverslip using an automated imaging pipeline created in NIS
564 elements or the samples were blinded prior to imaging. A minimum of five Z-stacks were
565 collected per coverslip with 0.25 µm step size. To display representative images, all slices
566 within a stack were collapsed into a single image based upon the maximum intensity of
567 pixels in each slice using NIS elements software.

568 **Intensity Analysis:**

569 The signal intensity of random spots of synaptopodin, actin, mDia, Arp2, N-WASP, α-
570 actinin-4 and myosin IIb around bacteria was measured using NIS elements. Three spots
571 were analyzed at each bacterium, and 5-30 bacteria were measured per condition per
572 experiment, and the average intensity was recorded per experiment.

573 **Statistical Analysis:**

574 Statistical difference between means was analyzed with Graph Pad Prism 9. Statistical
575 difference of two means was determined either by Student's t-test or a paired t-test.
576 Unless indicated otherwise, the differences between the means of multiple groups were
577 determined either by two-way ANOVA with Sidak *post hoc* test or by one-way ANOVA
578 with either a Holm-Sidak's *post hoc* test or a Dunnett's *post hoc* test.

579

580 **Acknowledgements**

581 We would like to thank Marcia Goldberg, Vivian Tang, Cammie Lesser, and Hervé
582 Agaisse for reagents. We would like to thank Marcia Goldberg, Cristina Penaranda, Lilian
583 Radoshevich, Marijke Keestra-Gounder and the Keestra-Gounder lab for helpful
584 discussions. We would like to thank Tinalyn Kupfer and the CU | AMC ImmunoMicro Flow
585 Cytometry Shared Resource, RRID:SCR_021321, for assistance with cell sorting. This
586 work was funded by K22 AI137296, the GI and Liver Innate Immune Program at the
587 University of Colorado, and the University of Colorado start-up funds to BCR. JER was
588 funded by T32 AI052066.

589 **Author Contributions**

590 J.M.V and B.C.R wrote the initial draft of the manuscript. J.M.V, D.J.H, T.B.H, T.N.H.
591 S.P.C., L.L.L., and B.C.R designed experiments. J.M.V, J.D.T, B.C.R, D.J.H, T.B.H,
592 T.N.H. L.Z.,and J.E.R preformed experiments. All authors discussed the results and
593 commented on the manuscript.

594

COMPETING FINANCIAL INTEREST

The authors declare no competing financial interest.

598 **REFERENCES**

599 1. Dhanda AS, Guttman JA. 2022. Localization of host endocytic and actin-
600 associated proteins during Shigella flexneri intracellular motility and intercellular
601 spreading. Anat Rec (Hoboken) doi:10.1002/ar.24955.
602 2. Stevens JM, Galyov EE, Stevens MP. 2006. Actin-dependent movement of
603 bacterial pathogens. Nat Rev Microbiol 4:91-101.
604 3. Hiller G, Weber K, Schneider L, Parajsz C, Jungwirth C. 1979. Interaction of
605 assembled progeny pox viruses with the cellular cytoskeleton. Virology 98:142-
606 53.
607 4. Lamason RL, Welch MD. 2017. Actin-based motility and cell-to-cell spread of
608 bacterial pathogens. Curr Opin Microbiol 35:48-57.
609 5. Weddle E, Agaisse H. 2018. Principles of intracellular bacterial pathogen spread
610 from cell to cell. PLoS Pathog 14:e1007380.
611 6. Agaisse H. 2016. Molecular and Cellular Mechanisms of Shigella flexneri
612 Dissemination. Front Cell Infect Microbiol 6:29.
613 7. Hale TL. 1991. Genetic basis of virulence in Shigella species. Microbiol Rev
614 55:206-24.
615 8. Labrec EH, Schneider H, Magnani TJ, Formal SB. 1964. Epithelial Cell
616 Penetration as an Essential Step in the Pathogenesis of Bacillary Dysentery. J
617 Bacteriol 88:1503-18.
618 9. Goldberg MB, Barzu O, Parsot C, Sansonetti PJ. 1993. Unipolar localization and
619 ATPase activity of IcsA, a Shigella flexneri protein involved in intracellular
620 movement. Infect Agents Dis 2:210-1.

621 10. Egile C, Loisel TP, Laurent V, Li R, Pantaloni D, Sansonetti PJ, Carlier MF. 1999.
622 Activation of the CDC42 effector N-WASP by the Shigella flexneri IcsA protein
623 promotes actin nucleation by Arp2/3 complex and bacterial actin-based motility. J
624 Cell Biol 146:1319-32.
625 11. Bernardini ML, Mounier J, d'Hauteville H, Coquis-Rondon M, Sansonetti PJ.
626 1989. Identification of icsA, a plasmid locus of Shigella flexneri that governs
627 bacterial intra- and intercellular spread through interaction with F-actin. Proc Natl
628 Acad Sci U S A 86:3867-71.
629 12. Kadurugamuwa JL, Rohde M, Wehland J, Timmis KN. 1991. Intercellular spread
630 of Shigella flexneri through a monolayer mediated by membranous protrusions
631 and associated with reorganization of the cytoskeletal protein vinculin. Infect
632 Immun 59:3463-71.
633 13. Campbell-Valois FX, Sachse M, Sansonetti PJ, Parsot C. 2015. Escape of
634 Actively Secreting Shigella flexneri from ATG8/LC3-Positive Vacuoles Formed
635 during Cell-To-Cell Spread Is Facilitated by IcsB and VirA. mBio 6:e02567-14.
636 14. Sansonetti PJ, Arondel J, Fontaine A, d'Hauteville H, Bernardini ML. 1991. OmpB
637 (osmo-regulation) and icsA (cell-to-cell spread) mutants of Shigella flexneri:
638 vaccine candidates and probes to study the pathogenesis of shigellosis. Vaccine
639 9:416-22.
640 15. Suzuki T, Sasakawa C. 2001. Molecular basis of the intracellular spreading of
641 Shigella. Infect Immun 69:5959-66.

642 16. Yum LK, Byndloss MX, Feldman SH, Agaisse H. 2019. Critical role of bacterial
643 dissemination in an infant rabbit model of bacillary dysentery. Nat Commun
644 10:1826.
645 17. Mitchell PS, Roncaioli JL, Turcotte EA, Goers L, Chavez RA, Lee AY, Lesser CF,
646 Rauch I, Vance RE. 2020. NAIP-NLRC4-deficient mice are susceptible to
647 shigellosis. Elife 9.
648 18. Chriett S, Dabek A, Wojtala M, Vidal H, Balcerczyk A, Pirola L. 2019. Prominent
649 action of butyrate over beta-hydroxybutyrate as histone deacetylase inhibitor,
650 transcriptional modulator and anti-inflammatory molecule. Sci Rep 9:742.
651 19. Singh V, Lee G, Son H, Koh H, Kim ES, Unno T, Shin JH. 2022. Butyrate
652 producers, "The Sentinel of Gut": Their intestinal significance with and beyond
653 butyrate, and prospective use as microbial therapeutics. Front Microbiol
654 13:1103836.
655 20. Lozupone CA, Stombaugh JI, Gordon JI, Jansson JK, Knight R. 2012. Diversity,
656 stability and resilience of the human gut microbiota. Nature 489:220-30.
657 21. Ornelas A, Welch N, Countess JA, Zhou L, Wang RX, Dowdell AS, Colgan SP.
658 2023. Mimicry of microbially-derived butyrate reveals templates for potent
659 intestinal epithelial HIF stabilizers. Gut Microbes 15:2267706.
660 22. Wang RX, Henen MA, Lee JS, Vogeli B, Colgan SP. 2021. Microbiota-derived
661 butyrate is an endogenous HIF prolyl hydroxylase inhibitor. Gut Microbes
662 13:1938380.

663 23. Wang RX, Lee JS, Campbell EL, Colgan SP. 2020. Microbiota-derived butyrate
664 dynamically regulates intestinal homeostasis through regulation of actin-
665 associated protein synaptopodin. Proc Natl Acad Sci U S A 117:11648-11657.
666 24. Morris T, Sue E, Geniesse C, Brieher WM, Tang VW. 2022. Synaptopodin stress
667 fiber and contractomere at the epithelial junction. J Cell Biol 221.
668 25. Robbins JR, Barth AI, Marquis H, de Hostos EL, Nelson WJ, Theriot JA. 1999.
669 Listeria monocytogenes exploits normal host cell processes to spread from cell to
670 cell. J Cell Biol 146:1333-50.
671 26. Ichimura K, Kurihara H, Sakai T. 2003. Actin filament organization of foot
672 processes in rat podocytes. J Histochem Cytochem 51:1589-600.
673 27. Yap K, Drakew A, Smilovic D, Rietsche M, Paul MH, Vuksic M, Del Turco D,
674 Deller T. 2020. The actin-modulating protein synaptopodin mediates long-term
675 survival of dendritic spines. Elife 9.
676 28. Heindl JE, Saran I, Yi CR, Lesser CF, Goldberg MB. 2010. Requirement for
677 formin-induced actin polymerization during spread of Shigella flexneri. Infect
678 Immun 78:193-203.
679 29. Fattouh R, Kwon H, Czuczman MA, Copeland JW, Pelletier L, Quinlan ME,
680 Muise AM, Higgins DE, Brumell JH. 2015. The diaphanous-related formins
681 promote protrusion formation and cell-to-cell spread of Listeria monocytogenes. J
682 Infect Dis 211:1185-95.
683 30. Bishai EA, Sidhu GS, Li W, Dhillon J, Bohil AB, Cheney RE, Hartwig JH,
684 Southwick FS. 2013. Myosin-X facilitates Shigella-induced membrane
685 protrusions and cell-to-cell spread. Cell Microbiol 15:353-367.

686 31. Dragoi AM, Agaisse H. 2014. The serine/threonine kinase STK11 promotes
687 Shigella flexneri dissemination through establishment of cell-cell contacts
688 competent for tyrosine kinase signaling. Infect Immun 82:4447-57.
689 32. Monack DM, Theriot JA. 2001. Actin-based motility is sufficient for bacterial
690 membrane protrusion formation and host cell uptake. Cell Microbiol 3:633-47.
691 33. Theriot JA, Mitchison TJ, Tilney LG, Portnoy DA. 1992. The rate of actin-based
692 motility of intracellular Listeria monocytogenes equals the rate of actin
693 polymerization. Nature 357:257-60.
694 34. Gerbal F, Chaikin P, Rabin Y, Prost J. 2000. An elastic analysis of Listeria
695 monocytogenes propulsion. Biophys J 79:2259-75.
696 35. Giardini PA, Fletcher DA, Theriot JA. 2003. Compression forces generated by
697 actin comet tails on lipid vesicles. Proc Natl Acad Sci U S A 100:6493-8.
698 36. Buvall L, Rashmi P, Lopez-Rivera E, Andreeva S, Weins A, Wallentin H, Greka
699 A, Mundel P. 2013. Proteasomal degradation of Nck1 but not Nck2 regulates
700 RhoA activation and actin dynamics. Nat Commun 4:2863.
701 37. Moreau V, Frischknecht F, Reckmann I, Vincentelli R, Rabut G, Stewart D, Way
702 M. 2000. A complex of N-WASP and WIP integrates signalling cascades that
703 lead to actin polymerization. Nat Cell Biol 2:441-8.
704 38. Schuch R, Sandlin RC, Maurelli AT. 1999. A system for identifying post-invasion
705 functions of invasion genes: requirements for the Mxi-Spa type III secretion
706 pathway of Shigella flexneri in intercellular dissemination. Mol Microbiol 34:675-
707 89.

708 39. Duncan-Lowey JK, Wiscovitch AL, Wood TE, Goldberg MB, Russo BC. 2020.
709 Shigella flexneri Disruption of Cellular Tension Promotes Intercellular Spread.
710 Cell Rep 33:108409.
711 40. Kuehl CJ, Dragoi AM, Agaisse H. 2014. The Shigella flexneri type 3 secretion
712 system is required for tyrosine kinase-dependent protrusion resolution, and
713 vacuole escape during bacterial dissemination. PLoS One 9:e112738.
714 41. Nasser A, Mosadegh M, Azimi T, Shariati A. 2022. Molecular mechanisms of
715 Shigella effector proteins: a common pathogen among diarrheic pediatric
716 population. Mol Cell Pediatr 9:12.
717 42. Ernst NH, Reeves AZ, Ramseyer JE, Lesser CF. 2018. High-Throughput
718 Screening of Type III Secretion Determinants Reveals a Major Chaperone-
719 Independent Pathway. mBio 9.
720 43. Gall TL, Mavris M, Martino MC, Bernardini ML, Denamur E, Parsot C. 2005.
721 Analysis of virulence plasmid gene expression defines three classes of effectors
722 in the type III secretion system of Shigella flexneri. Microbiology (Reading)
723 151:951-962.
724 44. Kane CD, Schuch R, Day WA, Jr., Maurelli AT. 2002. MxiE regulates intracellular
725 expression of factors secreted by the Shigella flexneri 2a type III secretion
726 system. J Bacteriol 184:4409-19.
727 45. Hall CP, Jadeja NB, Sebeck N, Agaisse H. 2022. Characterization of MxiE- and
728 H-NS-Dependent Expression of ipaH7.8, ospC1, yccE, and yfdF in Shigella
729 flexneri. mSphere 7:e0048522.

730 46. Kelly CJ, Zheng L, Campbell EL, Saeedi B, Scholz CC, Bayless AJ, Wilson KE,
731 Glover LE, Kominsky DJ, Magnuson A, Weir TL, Ehrentraut SF, Pickel C, Kuhn
732 KA, Lanis JM, Nguyen V, Taylor CT, Colgan SP. 2015. Crosstalk between
733 Microbiota-Derived Short-Chain Fatty Acids and Intestinal Epithelial HIF
734 Augments Tissue Barrier Function. Cell Host Microbe 17:662-71.
735 47. Tinevez JY, Arena ET, Anderson M, Nigro G, Injarabian L, Andre A, Ferrari M,
736 Campbell-Valois FX, Devin A, Shorte SL, Sansonetti PJ, Marteyn BS. 2019.
737 Shigella-mediated oxygen depletion is essential for intestinal mucosa
738 colonization. Nat Microbiol 4:2001-2009.
739 48. Arena ET, Tinevez JY, Nigro G, Sansonetti PJ, Marteyn BS. 2017. The infectious
740 hypoxia: occurrence and causes during Shigella infection. Microbes Infect
741 19:157-165.
742 49. Vlachos A, Korkotian E, Schonfeld E, Copanaki E, Deller T, Segal M. 2009.
743 Synaptopodin regulates plasticity of dendritic spines in hippocampal neurons. J
744 Neurosci 29:1017-33.
745 50. Lum M, Morona R. 2014. Myosin IIA is essential for Shigella flexneri cell-to-cell
746 spread. Pathog Dis 72:174-87.
747 51. Moore AS, Coscia SM, Simpson CL, Ortega FE, Wait EC, Heddleston JM,
748 Nirschl JJ, Obara CJ, Guedes-Dias P, Boecker CA, Chew TL, Theriot JA,
749 Lippincott-Schwartz J, Holzbaur ELF. 2021. Actin cables and comet tails
750 organize mitochondrial networks in mitosis. Nature 591:659-664.

751 52. Erard M, Fredj A, Pasquier H, Beltolngar DB, Bousmah Y, Derrien V, Vincent P,
752 Merola F. 2013. Minimum set of mutations needed to optimize cyan fluorescent
753 proteins for live cell imaging. Mol Biosyst 9:258-67.
754 53. Eshleman EM, Bortell N, McDermott DS, Crisler WJ, Lenz LL. 2020. Myeloid cell
755 responsiveness to interferon-gamma is sufficient for initial resistance to Listeria
756 monocytogenes. Curr Res Immunol 1:1-9.
757 54. Weddle EA, Koseoglu VK, DeVasure BA, Agaisse HF. 2022. The type three
758 secretion system effector protein IpgB1 promotes Shigella flexneri cell-to-cell
759 spread through double-membrane vacuole escape. PLoS Pathog 18:e1010380.
760 55. Cole C, Thomas S, Filak H, Henson PM, Lenz LL. 2012. Nitric oxide increases
761 susceptibility of Toll-like receptor-activated macrophages to spreading Listeria
762 monocytogenes. Immunity 36:807-20.
763

764 **FIGURES**

765 **Figure 1: Butyrate promotes efficient *S. flexneri* intercellular spread.**

766 (A-B) Monolayers of T84 cells were infected with *S. flexneri* in the presence of 0 or 5 mM
767 butyrate, stained with neutral red at 48 hours of infection, and imaged. (A) Representative
768 images. Dotted lines show plaque boundary; scale bar, 0.6 mm. (B) Quantification of the
769 area of plaques from images represented in A, >50 plaques were measured per condition
770 per experiment. Dots are independent experiments. (C,D) T84 cells were treated with 0
771 or 5 mM butyrate for 24 hours, and Synaptopodin abundance was determined with
772 western blot. (B,D) ***, $p<0.001$; *, $p<0.05$ by paired t-test. Data are mean ± SEM.

773 **Figure 2: Synaptopodin is required for efficient intercellular spread of *S. flexneri***

774 Monolayers of T84 (A-B), MDCK (C-D), or HeLa (E-F) cells that produce a control or
775 synaptopodin specific shRNA were infected with *S. flexneri* and stained with neutral red
776 at 48 hours of infection. (A, C, and E) Representative images. Dotted lines indicate plaque
777 boundary. Scale bar, 0.5 mm. (B, D, and F) Quantification of the area of plaques from
778 images represented in A, C, and E. 15-60 plaques measured per condition per
779 experiment. Dots are independent experiments. *, $p<0.05$ by paired t-test (B and D) or by
780 one-way ANOVA with Dunnett's *post hoc* test (F). Data are mean ± SEM.

781 **Figure 3: Synaptopodin is required for protrusion formation by *S. flexneri***

782 (A) Representative images of HeLa cells infected with *S. flexneri.* Cyan, *S. flexneri;*
783 magenta, actin; blue, DNA. Arrows, bacteria in protrusions. Scale bar, 5 μM. 5-10 fields
784 were analyzed per condition per experiment. (B) Quantification of the percentage of

785 intracellular bacteria within a protrusion. (C) Quantification of the intensity of actin in
786 protrusions. (B and C) Dots are independent experiments. (D) Quantification of the length
787 of protrusions. Tukey method used to define whiskers. (B-D) N.S., not significant; *,
788 $p<0.05$ by one-way ANOVA with Holm-Sidak's *post hoc* test. (E-G) Time lapse images
789 from videos of bacteria forming plasma membrane protrusions. (E) Representative
790 images of protrusion formation. Cyan, S. *flexneri;* green, plasma membrane. Scale bar 5
791 μM. Arrows, bacteria in protrusions; dot, protrusion origination point; dotted line,
792 progression of protrusion formation. (F) Quantification of the speed of protrusion
793 formation from videos represented in E. (G) Quantification of the duration bacteria remain
794 in protrusions. (F-G) Dots are individual bacteria, pooled from 3 independent experiments.
795 *, $p<0.05$ by Student's t-test. Data are mean ± SEM.

796 **Figure 4: Synaptopodin regulates actin tail formation by *S. flexneri***

797 Infection of HeLa cells infected with *S. flexneri* for 90 min. (A) Representative images.
798 Cyan, *S. flexneri;* magenta, actin; blue, DNA. Arrows, bacteria with actin tails. Dotted line,
799 trace of actin tail. Scale bar, 5 μM. (B) Quantification of percentage of bacteria with actin
800 tails. (C) Quantification of the length of actin tails. (D-E) Time-lapsed microscopy of HeLa
801 cells producing a membrane anchored YFP infected with *S. flexneri* producing CFP. (D)
802 Representative still images from time-lapsed videos for 2 minutes from initial observation
803 of motility. Cyan, *S. flexneri*; green, plasma membrane. Dots are the position of bacteria
804 at each time point, dotted line is arbitrary straight line between dots showing bacterial
805 progression over time. Scale bar, 5 μM. (E) Quantification of the speed at which bacteria
806 move in the cytosol from videos represented in E. Mean indicated by bar. (B, C) 5-10
807 fields were analyzed per experiment. Dots are independent experiments. Data are mean

808 ± SEM. N.S., not significant; *, p<0.05; **, p<0.1; ***, p<0.001 by one-way ANOVA with
809 Dunnett's *post hoc* test. (E) N.S., not significant; *, p<0.05 by Student's t-test. Dots are
810 individual bacteria pooled together from three experiments. (F) Schematic depicting
811 shorter tails are formed in cells lacking synaptopodin compared to tails formed in control
812 cells. Generated with BioRender.

813 **Figure 5: Synaptopodin is required for myosin IIb recruitment around bacteria**

814 HeLa cells were infected with *S. flexneri* for 90 min. (A) Representative images. Cyan, *S.*
815 *flexneri*; magenta, actin; red, myosin IIb; blue, DNA. Arrows, bacteria with myosin IIb.
816 Scale bar, 5 μM. (B) Quantification of percentage of bacteria with myosin IIb. (C)
817 Quantification of the intensity of myosin IIb around bacteria. (D) Representative images
818 depicting α-actinin-4 recruitment around bacteria. Cyan, *S. flexneri;* magenta, actin; red,
819 α-actinin-4; blue, DNA. Arrows, bacteria with α-actinin-4. Scale bar, 5 μM. (E)
820 Quantification of the percentage of bacteria with α-actinin-4. (F) Quantification of the
821 intensity of α-actinin-4. (B-C and E-F) 5-10 fields were analyzed per condition per
822 experiment. Dots are independent experiments. Data are mean ± SEM. NS, not
823 significant; *, p<0.05; **, p<0.01 by one-way ANOVA with Dunnett's *post hoc* test.

824 **Figure 6: Synaptopodin is recruited around *S. flexneri* in an IcsA and a type 3**
825 **secretion system dependent manner**

826 Control HeLa cells were infected for 90 min with *S. flexneri* strains. (A) Representative
827 images. Cyan, *S. flexneri*; magenta, actin; red, synaptopodin (synpo); blue, DNA. Arrows,
828 bacteria with actin and synaptopodin. Scale bar, 5 μM. (B) Quantification of the

829 percentage of bacteria with actin. (C) Quantification of the percentage of bacteria with
830 synaptopodin. (D) Quantification of the intensity of actin around bacteria. (E)
831 Quantification of intensity of synaptopodin around bacteria. (B-E) 5-10 fields were
832 analyzed per condition per experiment. Dots are independent experiments. Data are
833 mean ± SEM. N.D., not detected. NS, not significant; *, $p<0.05$; **, $p<0.01$ by one-way
834 ANOVA with Dunnett's *post hoc* test.

835 **Figure 7. Schematic of *S. flexneri* intercellular spread in control versus**
836 **synaptopodin knockdown cell lines.**

837 Schematic of *S. flexneri* intercellular lifecycle. (I) *S. flexneri* induces its uptake into cells.
838 (II) Following uptake, it is present in a vacuole. (III) It escapes the vacuole into the cytosol
839 where the bacteria replicate. A portion of the bacteria nucleate the polymerization of actin,
840 which enables the bacteria to move in the cell cytosol. (V) Bacteria near the cell periphery
841 deform the plasma membrane into a protrusion. (VI) The protrusion resolves into a double
842 membrane vacuole. (VII) The bacteria escape the double membrane vacuole into the
843 cytosol. (A) Cells with synaptopodin enabled bacteria to form actin tails that are longer
844 and more aligned with the bacteria than cells lacking synaptopodin. Bacteria in cells with
845 synaptopodin form protrusions at a higher velocity that resolve more quickly (V). (B) In
846 cells lacking synaptopodin, the actin tails are shorter. Protrusions are formed at a slower
847 velocity and take longer to resolve into a double membrane vacuole (V). (A-B) 1. Bacteria
848 lacking IcsA do not polymerize actin or recruit synaptopodin. 2. Polar localization of IcsA
849 is associated with synaptopodin recruitment, and IcsA recruits N-WASP and Apr2/3
850 irrespective of synaptopodin abundance in cells. 3. Synaptopodin recruitment to bacteria
851 is further enhanced in a type 3 secretion dependent manner. Created with biorender.com

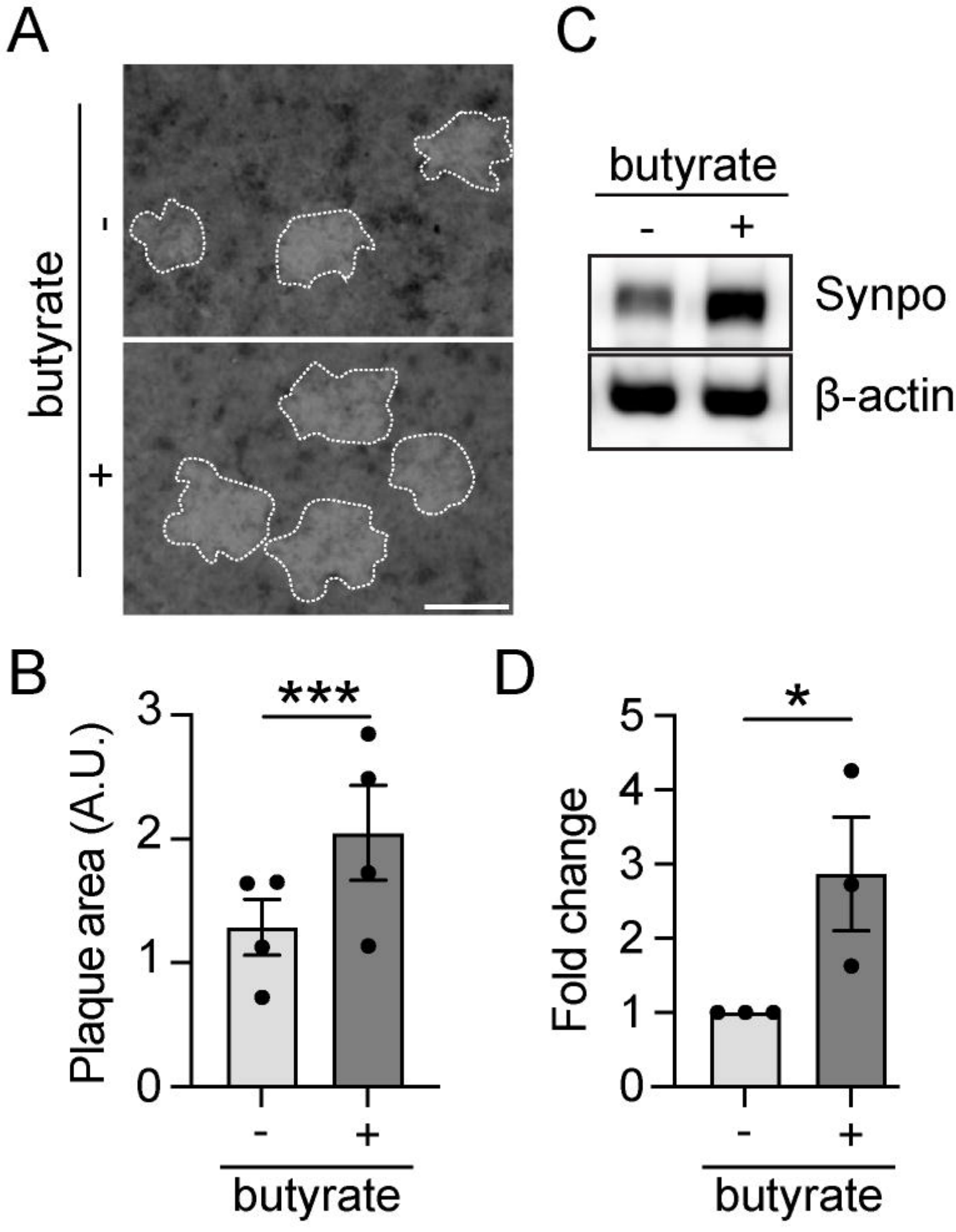
A
butyrate
-
+
C
butyrate
-
+
Synpo
β-actin
B
***
Plaque area (A.U.)
0
1
2
3
-
+
butyrate
D
*
Fold change
0
1
2
3
4
5
-
+
butyrate

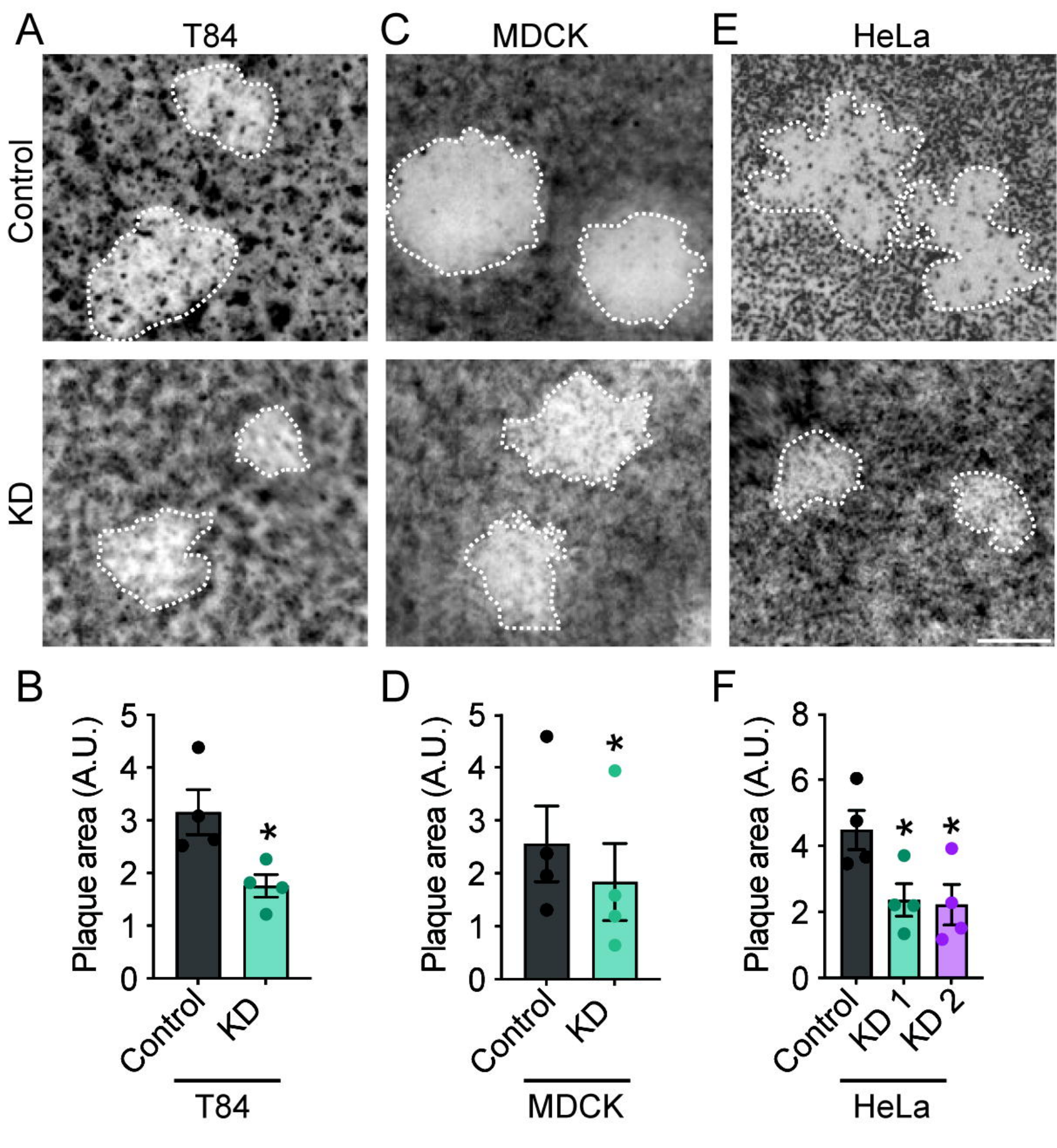
A
T84
C
MDCK
E
HeLa
Control
KD
B
Plaque area (A.U.)
5
4
3
2
1
0
*
Control
KD
T84
D
Plaque area (A.U.)
5
4
3
2
1
0
*
Control
KD
MDCK
F
Plaque area (A.U.)
8
6
4
2
0
*
*
Control
KD 1
KD 2
HeLa

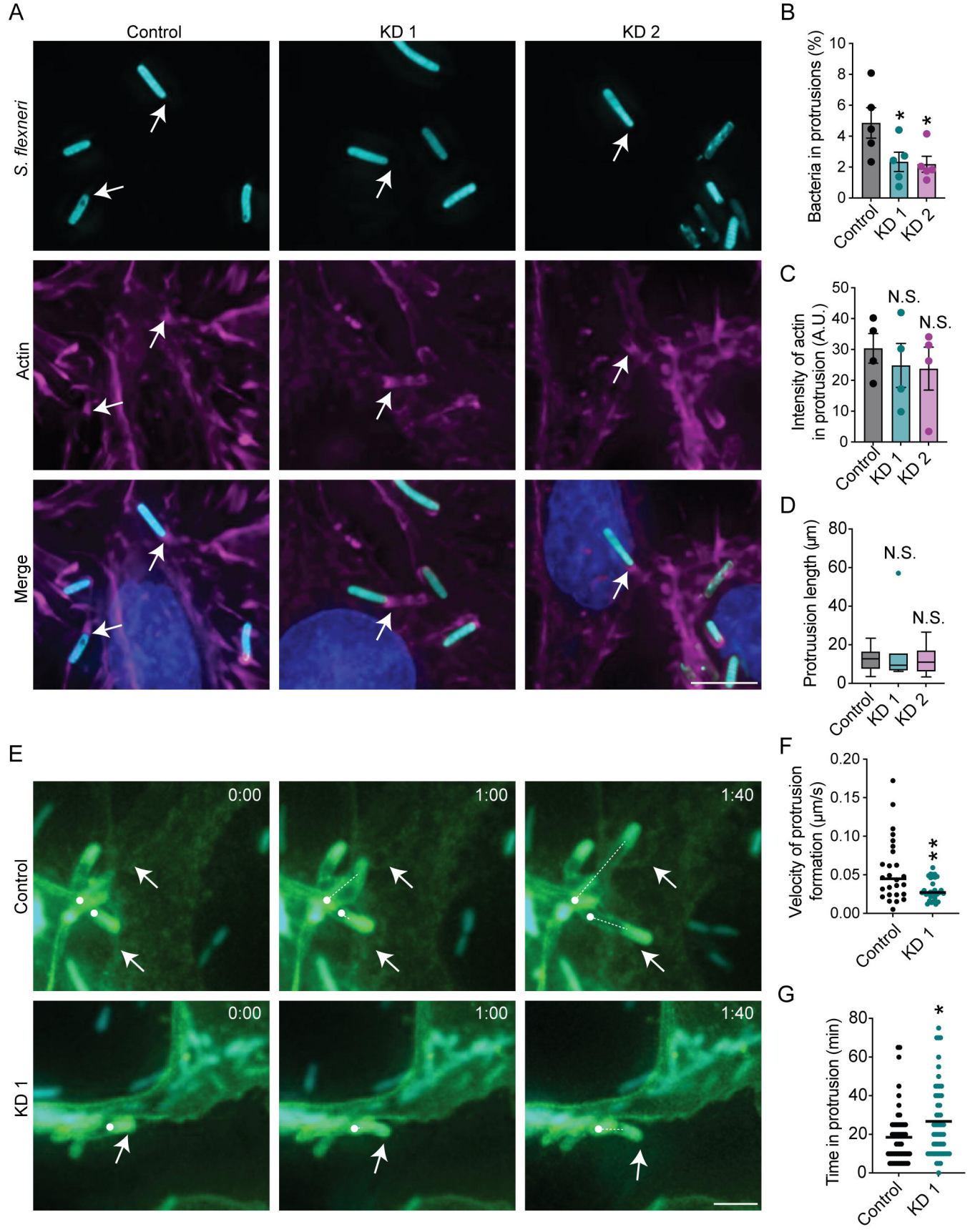
A
Control
KD 1
KD 2
S. flexneri
Actin
Merge
B
Bacteria in protrusions (%)
Control
KD 1
KD 2
C
Intensity of actin in protrusion (A.U.)
N.S.
N.S.
D
Protruusion length (µm)
N.S.
N.S.
E
0:00
1:00
1:40
Control
KD 1
F
Velocity of protrusion formation (µm/s)
G
Time in protrusion (min)

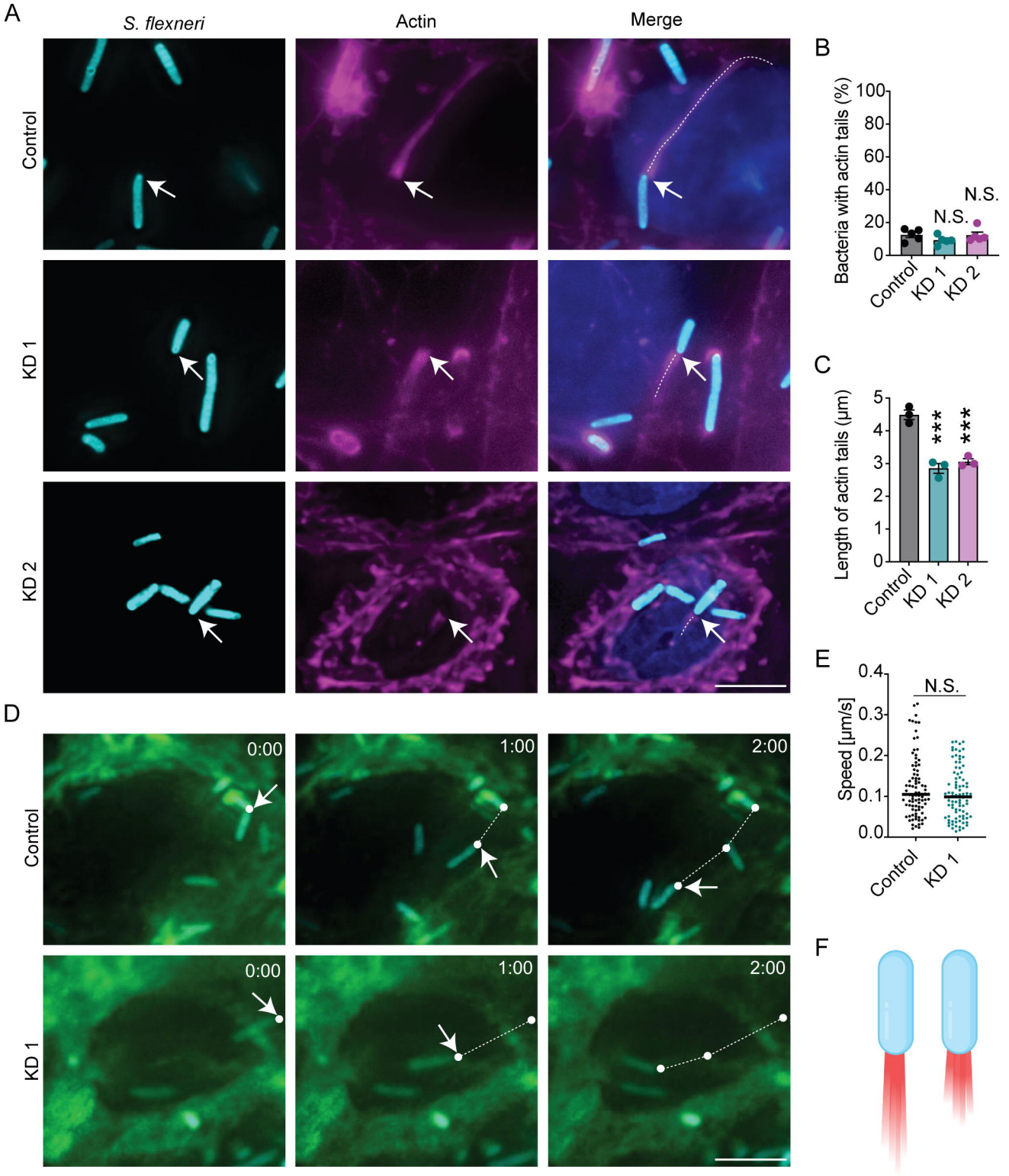
A
S. flexneri
Actin
Merge
Control
KD 1
KD 2
B
Bacteria with actin tails (%)
100
80
60
40
20
0
N.S.
N.S.
Control
KD 1
KD 2
C
Length of actin tails (µm)
5
4
3
2
1
0
***
***
Control
KD 1
KD 2
D
0:00
1:00
2:00
Control
KD 1
E
Speed [µm/s]
0.4
0.3
0.2
0.1
0.0
N.S.
Control
KD 1
F

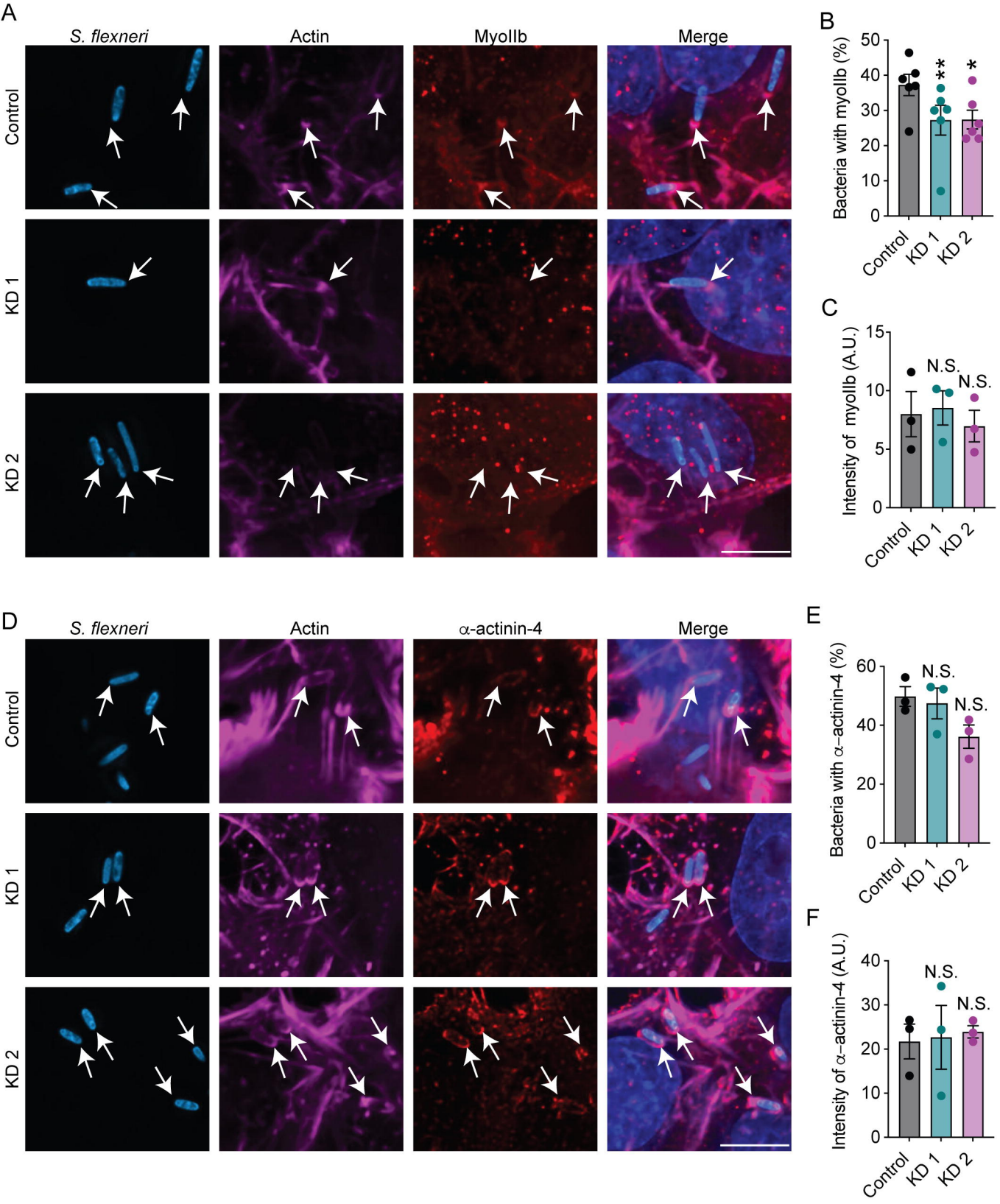
A
S. flexneri
Actin
MyoIIb
Merge
Control
KD 1
KD 2
B
Bacteria with myoIIb (%)
50
40
30
20
10
0
**
*
Control
KD 1
KD 2
C
Intensity of myoIIb (A.U.)
15
10
5
0
N.S.
N.S.
Control
KD 1
KD 2
D
S. flexneri
Actin
α-actinin-4
Merge
Control
KD 1
KD 2
E
Bacteria with α-actinin-4 (%)
60
40
20
0
N.S.
N.S.
Control
KD 1
KD 2
F
Intensity of α-actinin-4 (A.U.)
40
30
20
10
0
N.S.
N.S.
Control
KD 1
KD 2

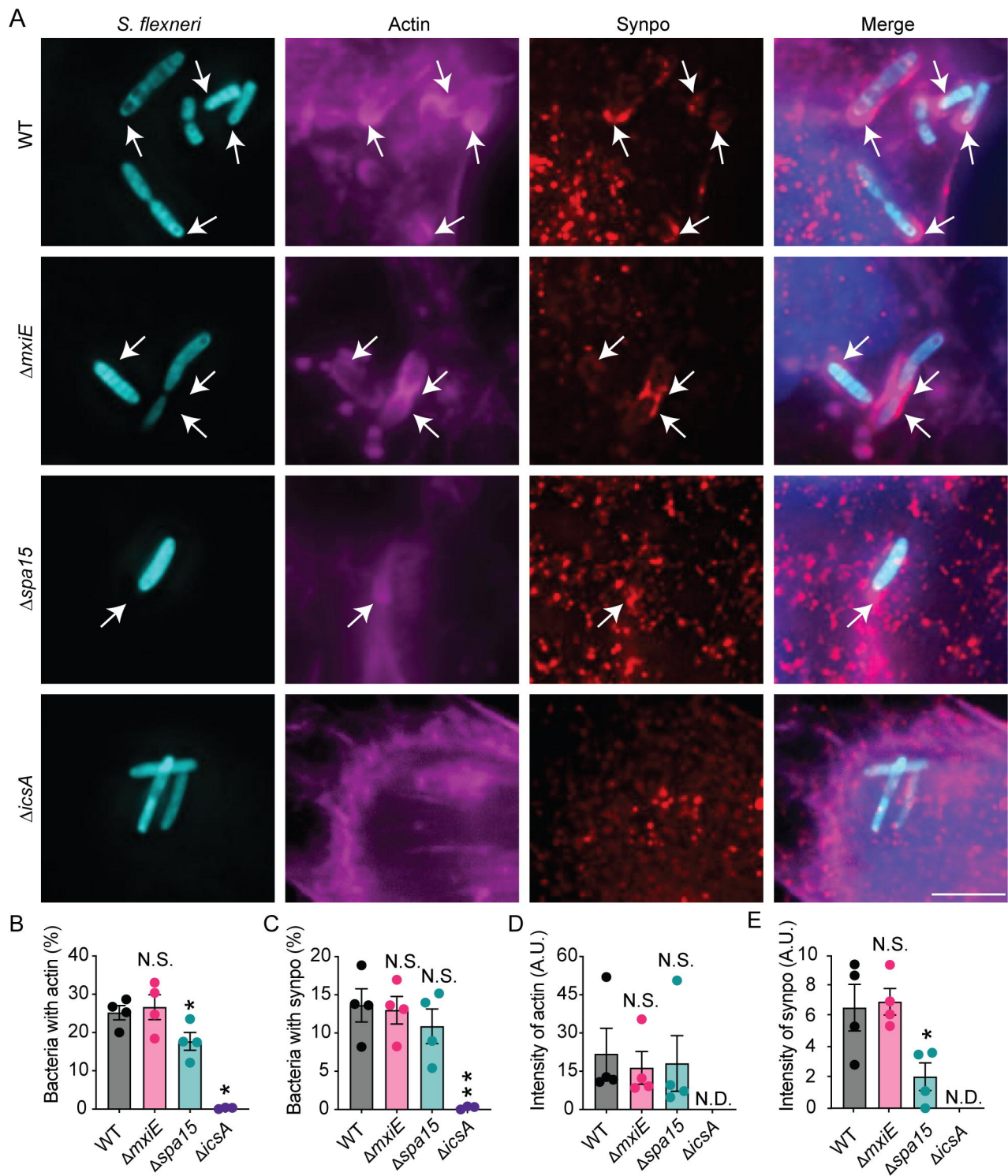
A
S. flexneri
Actin
Synpo
Merge
WT
ΔmxiE
Δspa15
ΔicsA
B
Bacteria with actin (%)
N.S.
*
*
C
Bacteria with synpo (%)
N.S.
N.S.
*
*
D
Intensity of actin (A.U.)
N.S.
N.S.
N.D.
E
Intensity of synpo (A.U.)
N.S.
*
N.D.
WT
ΔmxiE
Δspa15
ΔicsA

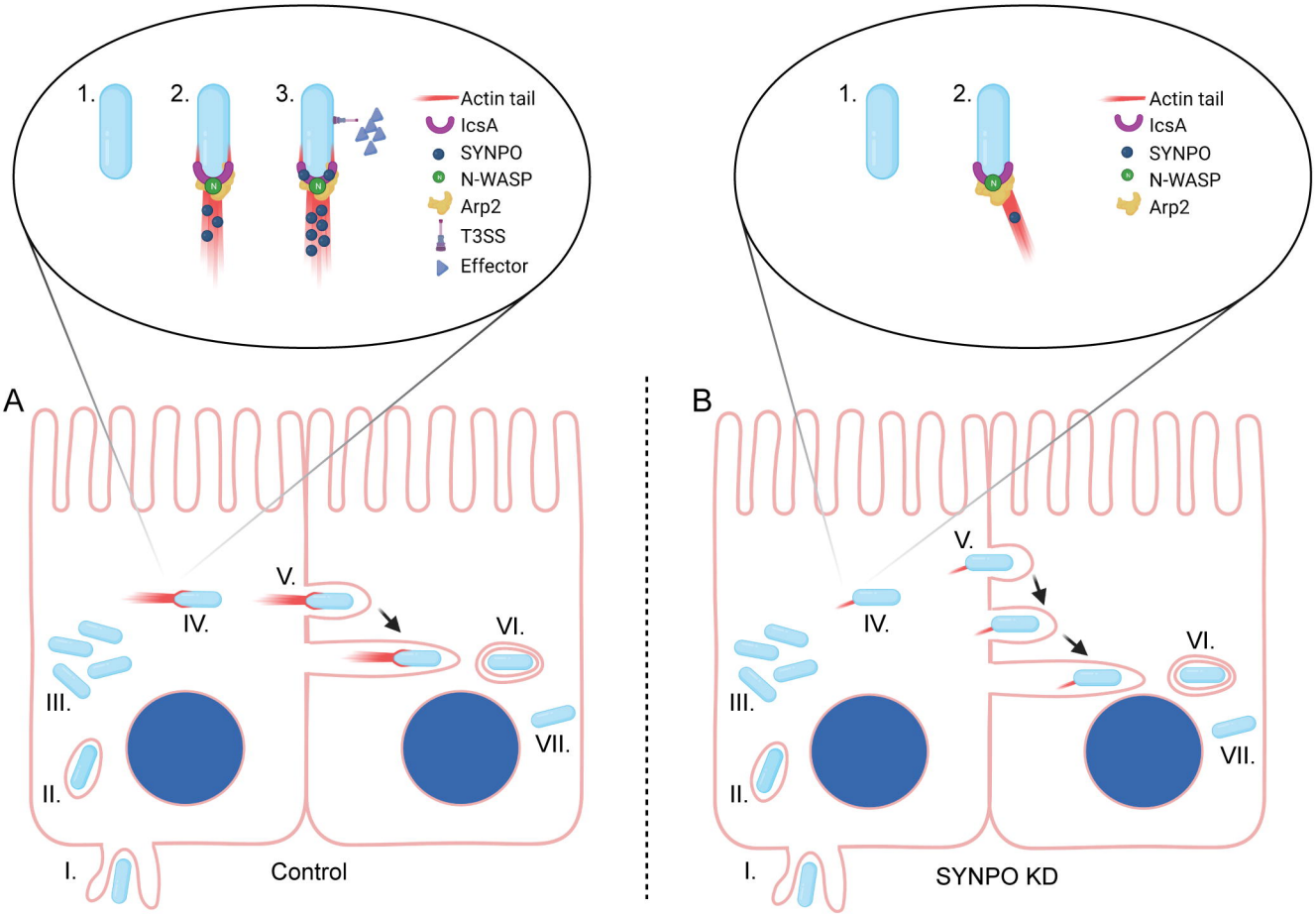
1.
2.
3.
Actin tail
IcsA
SYNPO
N-WASP
Arp2
T3SS
Effector
A
I.
II.
III.
IV.
V.
VI.
VII.
Control
B
1.
2.
Actin tail
IcsA
SYNPO
N-WASP
Arp2
I.
II.
III.
IV.
V.
VI.
VII.
SYNPO KD